**Journal of Sciences, Islamic Republic of Iran 29(2): 157 - 171 (2018)** http://jsciences.ut.ac.ir
University of Tehran, ISSN 1016-1104

# Petrography and Geochemistry of the Upper Jurassic Siliciclastic Rocks Equivalent to the Mozduran Gas Reservoir in the Eastern Kopet-Dagh Basin, NE Iran

H. Zand-Moghadam[1*], M. Jafarzadeh[2], R. Moussavi-Harami[3], A. Mahboubi[3]

[1] *Department of Geology, Faculty of Sciences, Shahid Bahonar University of Kerman, Kerman, Islamic Republic of Iran*
[2] *Faculty of Geosciences, Shahrood University of Technology, Shahrood, Shahrood, Islamic Republic of Iran*
[3] *Department of Geology, Faculty of Sciences, Ferdowsi University of Mashhad, Mashhad, Islamic Republic of Iran*

Received: 12 February 2017 / Revised: 14 May 2017 / Accepted: 3 July 2017

## Abstract

In this research, petrographic and geochemical (major and trace elements) characteristics of siliciclastic rocks of the Mozduran Formation in the eastern Kopet-Dagh Basin have been carried out in order to reveal their provenance such as source area paleoweathering, parent rock composition and tectonic setting. Mozduran Formation is mainly composed of limestone and dolomite, with minor amounts of siliciclastic rocks and evaporites. Siliciclastics rocks (sandstone and shale) of Mozduran Formation are mainly present in the easternmost parts of the Kopet-Dagh Basin. Four stratigraphic sections of Mozduran Formation, namely Kole-Malekabad, Kale-Karab, Deraz-Ab and Karizak, were measured and sampled in the SE of the basin. Petrographic investigation showed that the sandstones are mostly classifies as litharenite and feldspathic litharenite. Geochemical data revealed that CIA values of Mozduran siliciclastic rocks confirm a medium weathering that can be due to semi-arid climatic condition in the source area. Felsic composition of parent rocks and quatzolithic petrofacies of Mozduran Formation sandstones and their constituents such as Qp, Qm, Ls, Lm and F, together with paleocurrent analysis show that these siliciclastic sediments may have derived from uplifted and trusted belt of sedimentary or sedimentary-metamorphic rocks of south Mashhad and metamorphic rocks of north Fariman region. Petrographic and geochemical analyses suggest that these sediments deposited in a continental rifting system.

**Keywords:** Provenance; Siliciclastic; Geochemistry; Mozduran formation; Kopet-Dagh basin.

## Introduction

The Kopet-Dagh Basin of northeastern Iran formed after Middle Triassic, Early Cimmerian orogeny corresponding to the closure of the ancient Paleotethys Ocean [1]. The Khangiran and Gonbadli gas fields in

* Corresponding author: Tel / Fax: +983433221452; Email: Zand1883@uk.ac.ir

NE Iran are located in the eastern Kopet-Dagh Basin. These gas fields produce from the Upper Jurassic carbonates (Mozduran Formation) and the Lower Cretaceous siliciclastics (Shurijeh Formation) reservoirs [1, 2]. Since Mozduran Formation (Oxfordian-Kimmeridgian) is the main hydrocarbon reservoir in the Kopet-Dagh Basin, it is economically very important to study this formation. Based on surface and subsurface studies [3, 4, 5], this formation is mainly composed of limestone and dolomite, with minor amounts of marl/shale, siliciclastics and evaporites. Siliciclastics facies, sandstone and shale, increases in the volume toward the east; however there are still a few data available about depositional environment of these facies [2, 6]. Keeping in mind that provenance studies of siliciclastic rocks reveal the composition and geological history of sediment source areas [e.g, 7, 8, 9], therefore it is necessary to understand the provenance of these siliciclastic sediments that may have a potential reservoir in the subsurface. Thus, the main purpose of this study is to understand the provenance, tectonic setting and paleoclimate of the siliciclastic rocks of Mozduran Formation that have not been studied in detail so far.

***Geological setting***

The Kopet-Dagh sedimentary basin extends from the east of the Caspian Sea to NE Iran, as well as into Turkmenistan and north Afghanistan. This basin occupies approximately an area of about 500 $km^2$ in northeastern Iran and southwest Turkmenistan [1]. Kopet-Dagh Basin formed in an extensional regime (post-collisional rifting event after Cimmerian orogeny) during the Early to Middle Jurassic time [10]. About 10 km-thick sedimentary sequence of Middle Jurassic to Tertiary in the eastern parts of the basin confirms that sedimentation was relatively continuous from Jurassic to Neogene time in the Iranian portion of the Kopet-Dagh Basin and these rocks uncomfortably overlie Palaeozoic (basement) and Triassic rocks [1]. Basement in the Kopet-Dagh Basin is exposed at Aghdarband area in the southeast and is composed of sedimentary, metamorphic and igneous rocks (Devonian to Triassic), which were intensely deformed during the Hercynian and Cimmerian orogenies [see 11, 12]. The sedimentation in this basin began with deposition of the Middle Jurassic Kashafrud Formation which overly unconformable on Triassic or older basement rocks [13, 14]. Toward the East of the basin, the Upper Jurassic Mozduran Formation, the main gas reservoir in the Kopet-Dagh Basin, directly overly the Kashafrud Formation. The boundary between the Mozduran and Kashafrud Formations in the easternmost parts of the basin is disconformable [6]; to the west, the contact is conformable and gradual with deeper-marine Bathonian to Oxfordian carbonates, shales/marls of the Chaman-Bid Formation [1] (Fig. 1). Toward the east, the Chaman Bid Formation disappears and the base of Mozduran Formation is Oxfordian in age [1], which probably implies a Callovian hiatus. The Mozduran Formation becomes younger from west to east, and changes to shallow marine dolomite, thin gypsum layers and siliciclastic rocks [2, 6] suggesting that the basin was shallower in the east than the west during deposition of this succession. The Upper boundary of the Mozduran Formation is disconformable and is overlain by Lower Cretaceous redbed siliciclastics of the Shurijeh Formation. The Mozduran Formation at the type section (in the Mozduran pass in eastern Kopet-Dagh) has a thickness of about 420 m [1] and consists of light-colored thick-bedded limestones and massive, porous dolomitic limestones and dolomites. These carbonate rocks were deposited in the carbonate ramp [3, 5]. The siliciclastic rocks, equivalent to carbonates in easternmost parts of the basin, have mainly been deposited in coastal environment [2]. So that, facies characteristics and paleocurrent patterns of Mozduran lithofacies in south of Aghdarband (stratigraphic sections in this study) show that these sediments were deposited in coastal environment influenced by tidal currents and waves [6]. As stated above, the main aim of this study is to evaluate a provenance signature of the siliciclastic rocks of the Mozduran Formation which useful to understand paleotectonics of this region.

## Materials and Methods

In this study, four stratigraphic sections of the Mozduran Formation have been measured in the SE Kopet-Dagh Basin, including Kole-Malekabad (N 35° 54' 15" and E 60° 42’ 23.1"), Kale-Karab( N 35° 52’ 09" and E 60° 55’ 06"), Deraz-Ab (N 35° 51’ 56" and E 60° 57' 35.9") and Karizak (N 35° 49’ 47" and E 61° 01’ 37") (Fig. 2). In these sections, 300 siliciclastic samples were collected. 32 sandstone thin sections were selected for detailed petrographic studies (point-counting). Counting of 300 to 400 grains per thin section was carried out by using Gazzi-Dickinson method. Then for classification, Folk [15] scheme was used. Detrital modal analysis of the studied sandstones are presented in Table 1. After petrographic analyses, twenty five fine- to medium-grained sandstone and ten shale samples were selected for geochemical analyses of the major and trace elements. Analyses were done using X-ray Fluorescence (XRF) spectrometry technique on fused beads in Kansaran Binaloud Laboratory, Iran. Geochemical

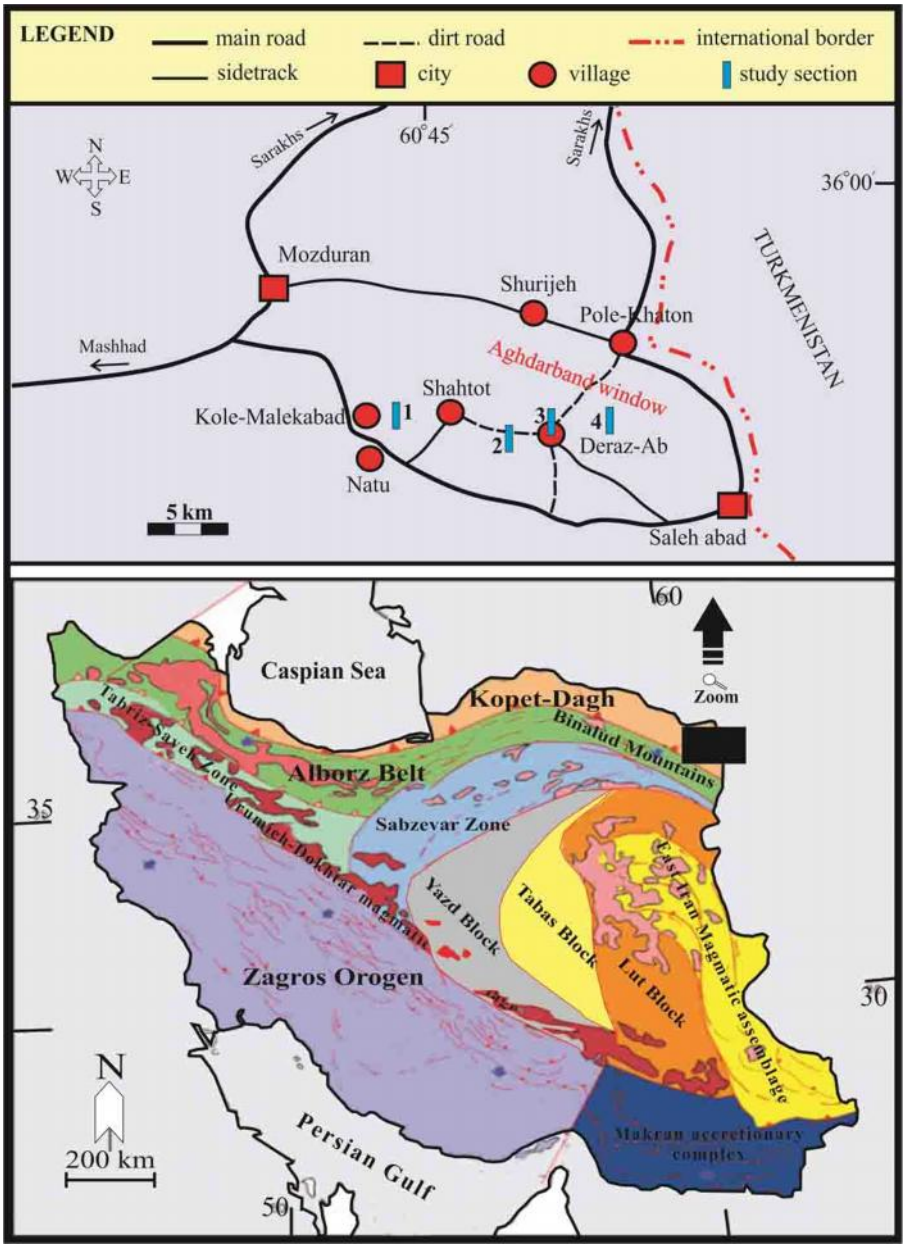


**Figure 1.** Location map of four stratigraphic section of Mozduran Formation at the south of Aghdarband area, SE Kopet-Dagh Basin.

results are presented in Tables 2 and 3.

## Results

### *1. Sandstone petrography*

Thirty two unaltered medium grained sandstone samples from 4 stratigraphic sections were selected for thin section analysis. Counting was performed for each thin section according to Gazzi-Dickinsson method. Point count data were recalculated and summarized in Table 1. The major constituents in these sandstones are quartz, feldspar and rock fragments, respectively. Quartz is the most abundant grain type and are mainly non-undulatory to slightly undulose monocrystalline quartz (60-80%) (Fig. 3A). Polycrystalline and metamorphic quartz are not abundant in Mozduran Formation sandstones (2 %) (Fig. 3B). Feldspars are dominantly K-feldspar and plagioclase (Fig. 3C-D). Potassium feldspars are mostly orthoclase, however microcline is also present as a minor amounts. K-feldspar is partially altered to clay minerals. The rock fragments are dominantly shale, chert and metamorphic

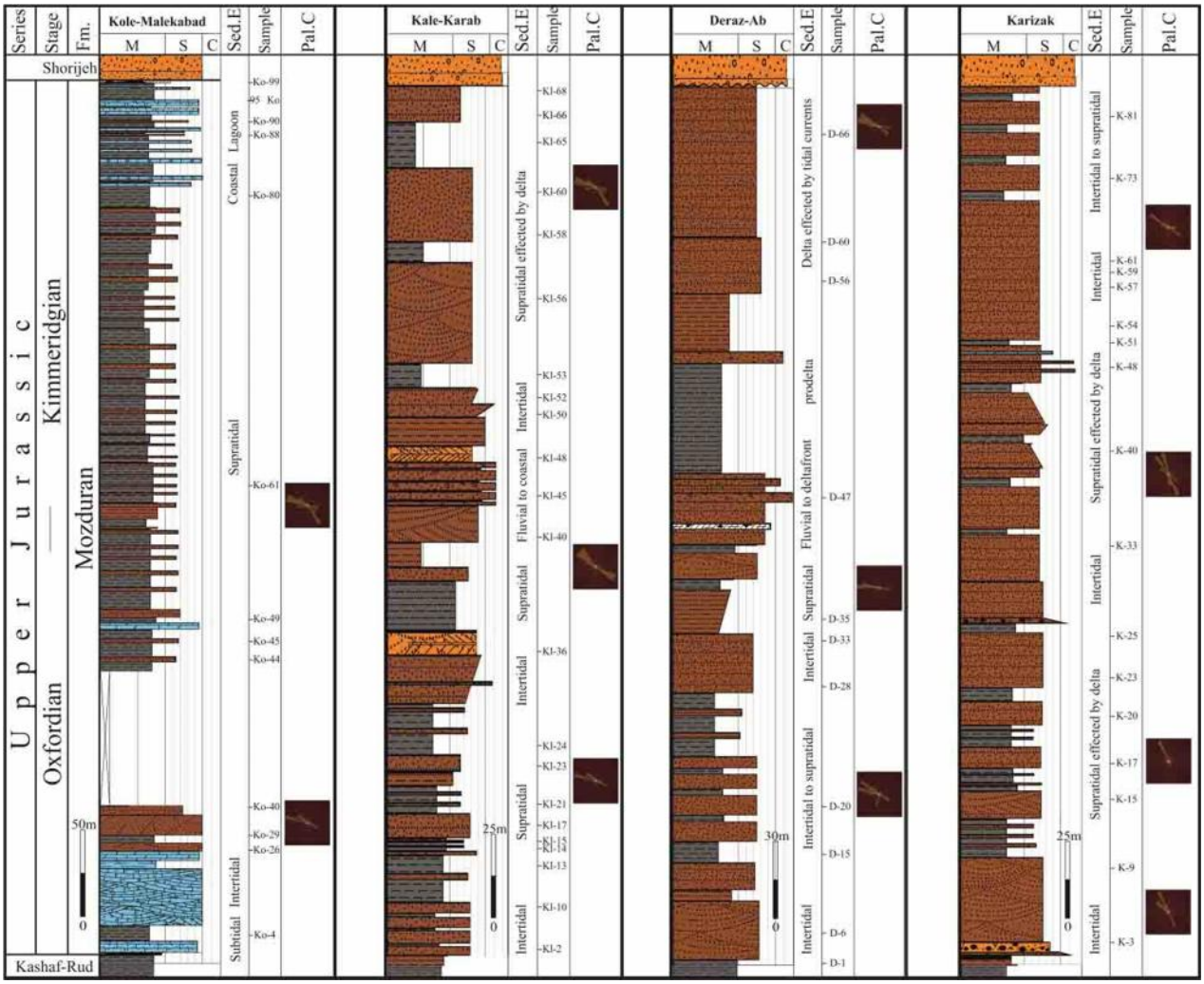


**Figure 2.** Stratigraphic column of the measured sections of Mozduran Formation and the location of samples in each section. Enviromental interpretation and paleocurrent analysis are modified from Zand-Moghadam et al. [6].

rock fragments with a few scattered volcanic particles (Fig. 3E-H). Muscovite, biotite, zircon and opaque minerals are the most accessory minerals in these sandstones (Fig. 3I). According to Folk [15] classification scheme, all samples are classified as litharenite and feldspathic litharenite (Fig. 4).

### *2. Geochemistry*

*1.2. Major element*

Results from analysis of 25 sandstone and 10 shale samples are presented in Table 2. The $SiO_2$ content in sandstone samples vary from 71.84 to 94.12 percent (average 81.92%) and from 54.07 wt% to 71.54 wt% (average 61.63 wt%) in shale samples. The $Al_2O_3$ concentration in sandstones and shales ranges from 2.51 wt% to 12.28 wt% (average 8.26 wt%) and from 13.70 wt% to 19.46 wt% (average 17.57 wt%), respectively. In comparsion of sandstone with shale samples, sandstones have higher concentration of $K_2O$ and $TiO_2$. The $K_2O$ content of sandstone ranges from 0.15 wt% to 3.29 wt% (average 2.01 wt%), while in shale samples ranges from 2.73 wt% to 5.18 wt% (average 4.24 wt%). The variation of $TiO_2$ content in sandstone samples are between 0.11 wt% to 0.62 wt% with the average of 0.37 wt%. It varies from 0.64 wt% to 0.95 wt% (average 0.81 wt%) in shale samples. Major elements of sandstone and shale samples were plotted on Harker's [16] variation diagrams against $Al_2O_3$ (Fig. 5). $SiO_2$ shows negatively correlation with $Al_2O_3$ (Fig. 5A). $Na_2O$ also shows a slightly negative correlation with $Al_2O_3$ (Fig. 5B). A positive correlation is evident between $Al_2O_3$ and $TiO_2$, and $Al_2O_3$ and $K_2O$ (Fig. 5 C-D), but CaO, MnO and MgO show poor correlations with $Al_2O_3$. The logarithmic relationship of $Fe_2O_3/K_2O$ versus

**Table 1.** Recalculated modal analysis of sandstones of Mozduran Formation (Ko: Kole-Malekabad section, Kl: Kale-Karab section, D: Deraz-Ab Section, K: Karizak Section).

| Sample No. | Qm F Lt (%) | | | Qt F L (%) | | | Q F RF (%) | | |
|---|---|---|---|---|---|---|---|---|---|
| | Qm | F | Lt | Qt | F | L | Q | F | RF |
| SST-Kl-10 | 55 | 4 | 42 | 70 | 4 | 26 | 57 | 4 | 39 |
| SST-Kl-15 | 60 | 8 | 32 | 79 | 8 | 13 | 65 | 8 | 27 |
| SST-Kl-21 | 56 | 5 | 39 | 78 | 5 | 17 | 58 | 5 | 36 |
| SST-Kl-36 | 60 | 4 | 36 | 76 | 4 | 20 | 63 | 4 | 33 |
| SST-Kl-45 | 56 | 3 | 41 | 76 | 3 | 20 | 65 | 3 | 32 |
| SST-Kl-52 | 52 | 8 | 40 | 69 | 8 | 23 | 57 | 8 | 34 |
| SST- Kl-68 | 29 | 0 | 71 | 89 | 0 | 11 | 74 | 0 | 26 |
| SST- D-6 | 60 | 4 | 36 | 72 | 4 | 24 | 63 | 4 | 33 |
| SST- D-20 | 71 | 4 | 25 | 83 | 4 | 13 | 60 | 4 | 36 |
| SST- D-28 | 54 | 4 | 42 | 66 | 4 | 30 | 71 | 4 | 25 |
| SST- D-33 | 56 | 5 | 39 | 68 | 5 | 27 | 54 | 4 | 42 |
| SST- D-47 | 37 | 5 | 58 | 48 | 5 | 47 | 59 | 5 | 36 |
| SST- D-56 | 52 | 2 | 45 | 71 | 2 | 27 | 42 | 5 | 52 |
| SST- D-66 | 61 | 4 | 35 | 79 | 4 | 18 | 65 | 2 | 33 |
| SST- K-3 | 19 | 2 | 79 | 67 | 2 | 31 | 61 | 4 | 35 |
| SST- K-9 | 51 | 5 | 44 | 74 | 5 | 22 | 48 | 2 | 49 |
| SST-K-17 | 46 | 4 | 50 | 71 | 4 | 25 | 57 | 5 | 39 |
| SST-K-23 | 47 | 5 | 47 | 74 | 5 | 20 | 53 | 4 | 43 |
| SST-K-33 | 53 | 3 | 44 | 71 | 3 | 27 | 57 | 3 | 40 |
| SST-K-40 | 58 | 2 | 40 | 77 | 2 | 21 | 62 | 2 | 36 |
| SST-K-48 | 47 | 5 | 47 | 82 | 5 | 12 | 59 | 5 | 35 |
| SST-K-57 | 55 | 5 | 40 | 70 | 5 | 25 | 55 | 5 | 40 |
| SST-K-73 | 66 | 4 | 30 | 78 | 4 | 18 | 66 | 4 | 30 |
| SST-Ko-26 | 68 | 5 | 27 | 83 | 5 | 12 | 67 | 5 | 28 |
| SST-Ko-29 | 49 | 13 | 38 | 65 | 13 | 23 | 74 | 4 | 22 |
| SST-Ko-40 | 55 | 7 | 38 | 69 | 7 | 24 | 77 | 3 | 20 |
| SST-Ko-44 | 58 | 6 | 37 | 79 | 6 | 15 | 72 | 3 | 24 |
| SST-Ko-45 | 44 | 4 | 52 | 58 | 4 | 38 | 72 | 6 | 22 |
| SST-Ko-61 | 46 | 6 | 48 | 63 | 6 | 31 | 64 | 5 | 31 |
| SST-Ko-88 | 66 | 6 | 28 | 80 | 6 | 14 | 60 | 7 | 33 |
| SST-Ko-90 | 68 | 6 | 26 | 82 | 6 | 12 | 58 | 6 | 36 |
| SST-Ko-95 | 54 | 5 | 41 | 73 | 5 | 22 | 60 | 10 | 30 |

$SiO_2/Al_2O_3$ in the Herron [17] diagram shows that the Mozduran sandstones can be classified as litharenite (Fig. 6).

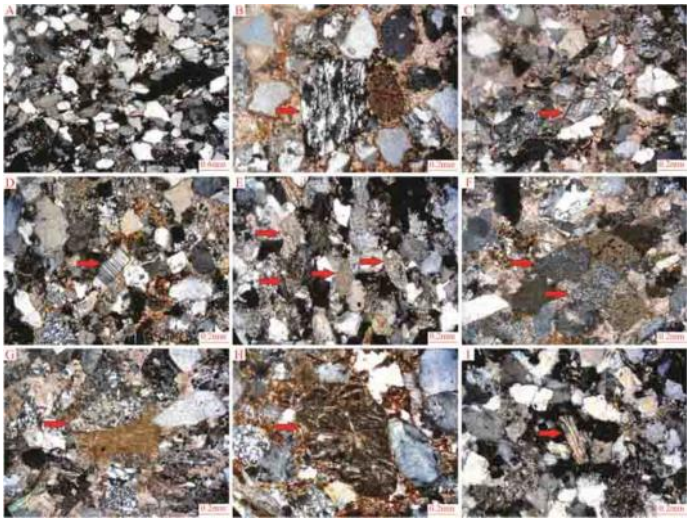

**Figure 3.** Photomicrograph of some selected sandstone samples: A) Non-undulatory to slightly undulose monocrystalline medium grained quartz, B) A stretched metamorphic grain quartz, C) A Microcline grain as one of K-feldspars, D) Plagioclase grain with albitic twins in sandstones at Karizak section, E) Some mudstone rock fragments (red arrows), F) Two grains of chert rock fragments (red arrows) in sandstones at Kole-Malek section, G) A metamorphic rock fragments (red arrow) at Karizak section, H) A rare volcanic rock fragments (microlithic texture) in sandstones, I) Muscovite grain as an accessory minerals in Mozduran Formation sandstones.

**Table 2.** Major element compositions of sandstone and mudstone samples

| Sample No. | $SiO_2$ | $TiO_2$ | $Al_2O_3$ | $Fe_2O_3$ | MnO | MgO | CaO | $Na_2O$ | $K_2O$ | $P_2O_5$ | LOI | CIA | PIA | ICV |
|---|---|---|---|---|---|---|---|---|---|---|---|---|---|---|
| SST-Kl-36 | 73.08 | 0.62 | 12.28 | 3.75 | 0.02 | 2.04 | 0.74 | 1.20 | 2.92 | 0.10 | 2.91 | 66.31 | 74.76 | 0.92 |
| SST-Kl-40 | 81.95 | 0.25 | 7.89 | 3.70 | 0.03 | 0.89 | 0.19 | 0.92 | 2.09 | 0.05 | 1.86 | 66.35 | 76.40 | 1.02 |
| SST-K48 | 84.38 | 0.26 | 7.33 | 2.31 | 0.02 | 0.70 | 0.16 | 1.46 | 1.60 | 0.04 | 1.44 | 62.88 | 68.32 | 0.89 |
| SST-Kl-50 | 83.39 | 0.30 | 7.41 | 2.76 | 0.01 | 0.67 | 0.18 | 1.19 | 1.98 | 0.05 | 1.75 | 63.24 | 70.87 | 0.96 |
| SST-K-56 | 75.00 | 0.62 | 10.95 | 3.64 | 0.02 | 1.61 | 0.60 | 1.26 | 2.63 | 0.07 | 3.13 | 65.21 | 73.01 | 0.95 |
| SST-Kl-60 | 75.54 | 0.57 | 10.80 | 4.04 | 0.03 | 1.73 | 0.53 | 1.23 | 2.58 | 0.09 | 2.57 | 66.00 | 74.29 | 0.99 |
| SST-Kl-66 | 80.07 | 0.45 | 9.93 | 2.11 | 0.01 | 1.30 | 0.33 | 1.27 | 2.44 | 0.05 | 1.81 | 65.59 | 73.94 | 0.80 |
| SST-K-20 | 71.84 | 0.58 | 11.99 | 4.35 | 0.03 | 2.12 | 0.85 | 1.43 | 2.89 | 0.10 | 3.35 | 63.86 | 70.78 | 1.02 |
| SST-D-28 | 78.21 | 0.51 | 10.71 | 1.92 | 0.01 | 1.29 | 0.49 | 1.17 | 2.78 | 0.12 | 2.29 | 65.92 | 75.29 | 0.76 |
| SST-D-35 | 76.34 | 0.34 | 10.76 | 3.39 | 0.03 | 1.42 | 0.59 | 1.11 | 3.29 | 0.05 | 2.44 | 62.93 | 72.15 | 0.94 |
| SST-D-60 | 82.83 | 0.31 | 8.26 | 2.31 | 0.03 | 0.79 | 0.24 | 1.74 | 1.86 | 0.04 | 1.41 | 61.30 | 66.11 | 0.88 |
| SST- K-15 | 76.08 | 0.57 | 10.88 | 3.36 | 0.04 | 1.76 | 0.32 | 1.30 | 2.61 | 0.08 | 2.37 | 67.02 | 76.11 | 0.91 |
| SST-K-25 | 80.25 | 0.37 | 9.51 | 2.46 | 0.04 | 1.04 | 0.60 | 1.27 | 2.35 | 0.07 | 1.82 | 63.12 | 69.82 | 0.85 |
| SST-K-40 | 81.79 | 0.38 | 8.71 | 2.53 | 0.03 | 1.07 | 0.34 | 1.11 | 2.18 | 0.08 | 1.57 | 65.38 | 73.82 | 0.87 |
| SST-K-54 | 84.51 | 0.26 | 6.96 | 1.75 | 0.03 | 0.65 | 0.77 | 1.66 | 1.54 | 0.10 | 1.60 | 55.60 | 57.64 | 0.95 |
| SST- K-59 | 86.02 | 0.28 | 6.53 | 2.05 | 0.04 | 0.41 | 0.12 | 1.00 | 1.52 | 0.04 | 1.25 | 65.68 | 73.44 | 0.82 |
| SST- K-61 | 82.92 | 0.36 | 7.50 | 3.00 | 0.04 | 0.71 | 0.31 | 1.40 | 1.81 | 0.06 | 1.69 | 61.57 | 67.06 | 1.01 |
| SST- K-81 | 87.35 | 0.23 | 6.29 | 1.74 | 0.00 | 0.24 | 0.12 | 1.33 | 1.49 | 0.05 | 1.00 | 61.74 | 67.17 | 0.82 |
| SST- Ko-29 | 94.12 | 0.11 | 2.51 | 0.98 | 0.00 | 0.17 | 0.25 | 0.21 | 0.15 | 0.01 | 1.15 | 74.63 | 77.27 | 0.75 |
| SST- Ko-99 | 91.80 | 0.28 | 3.36 | 2.04 | 0.01 | 0.49 | 0.17 | 0.16 | 0.51 | 0.02 | 0.97 | 75.74 | 84.27 | 1.09 |
| SST- Kl-2 | 81.70 | 0.47 | 8.14 | 2.50 | 0.01 | 0.46 | 0.31 | 1.12 | 2.26 | 0.06 | 2.61 | 63.36 | 71.57 | 0.87 |
| SST- Kl-17 | 84.56 | 0.26 | 7.09 | 1.84 | 0.01 | 0.75 | 0.37 | 1.07 | 1.85 | 0.14 | 1.62 | 63.36 | 70.81 | 0.87 |
| SST- Kl-23 | 83.93 | 0.33 | 7.24 | 2.30 | 0.01 | 0.62 | 0.67 | 0.98 | 2.00 | 0.04 | 1.66 | 59.64 | 64.99 | 0.95 |
| SST-Kl-56 | 87.63 | 0.16 | 5.59 | 2.01 | 0.02 | 0.64 | 0.17 | 1.04 | 1.30 | 0.04 | 1.17 | 62.66 | 68.50 | 0.95 |
| SST-Kl-58 | 82.67 | 0.46 | 7.90 | 3.08 | 0.01 | 0.60 | 0.21 | 1.32 | 1.64 | 0.04 | 1.80 | 65.12 | 71.37 | 0.93 |
| Mean | 81.92 | 0.37 | 8.72 | 2.64 | 0.02 | 0.97 | 0.37 | 1.12 | 2.16 | 0.06 | 1.89 | 64.59 | 71.59 | 0.91 |
| M-Kl-13 | 63.33 | 0.74 | 16.47 | 5.70 | 0.04 | 2.46 | 1.48 | 1.23 | 3.63 | 0.09 | 4.48 | 67.38 | 75.61 | 0.93 |
| M-Kl-14 | 71.54 | 0.64 | 13.70 | 2.07 | 0.01 | 1.08 | 0.08 | 1.22 | 3.31 | 0.04 | 4.97 | 70.84 | 83.11 | 0.61 |
| M-Kl-24 | 62.26 | 0.83 | 18.95 | 5.85 | 0.04 | 2.69 | 0.86 | 0.94 | 4.27 | 0.09 | 2.03 | 71.60 | 83.20 | 0.81 |
| M-Kl-65 | 58.13 | 0.94 | 19.17 | 6.93 | 0.02 | 2.15 | 0.58 | 0.44 | 5.18 | 0.08 | 4.53 | 73.10 | 90.36 | 0.85 |
| M- D-1 | 61.05 | 0.77 | 18.29 | 5.94 | 0.17 | 2.45 | 0.53 | 0.93 | 4.34 | 0.09 | 4.83 | 72.39 | 85.649 | 0.82 |
| M- D-15 | 58.22 | 0.80 | 18.63 | 6.86 | 0.05 | 3.34 | 0.62 | 0.80 | 4.63 | 0.09 | 5.57 | 72.02 | 85.944 | 0.92 |
| M- K-51 | 65.48 | 0.90 | 17.17 | 4.83 | 0.04 | 2.18 | 0.39 | 0.82 | 4.19 | 0.14 | 3.46 | 73.29 | 88.003 | 0.78 |
| M- Ko-4 | 56.69 | 0.78 | 19.46 | 6.16 | 0.04 | 2.18 | 1.83 | 0.38 | 4.97 | 0.11 | 6.99 | 74.59 | 91.847 | 0.84 |
| M- Ko-49 | 65.56 | 0.78 | 14.92 | 6.88 | 0.04 | 2.64 | 1.21 | 1.00 | 2.73 | 0.12 | 3.83 | 70.50 | 78.438 | 1.02 |
| M- Ko-80 | 54.07 | 0.95 | 18.95 | 9.48 | 0.04 | 3.04 | 1.18 | 0.16 | 5.11 | 0.15 | 6.45 | 75.77 | 96.224 | 1.05 |
| Mean | 61.63 | 0.81 | 17.57 | 6.07 | 0.05 | 2.42 | 0.88 | 0.79 | 4.24 | 0.10 | 4.71 | 70.83 | 85.84 | 0.86 |
| UCC | 66.60 | 0.64 | 15.40 | 5.04 | 0.10 | 2.48 | 3.59 | 3.27 | 2.80 | 0.15 | ---- | ---- | ---- | ---- |

*2.2.Trace elements*

The trace element concentrations and some elemental ratios of sandstone and shale are presented in Tables 3 and 4. Compared to the average Upper Continental Crust, The Mozduran Formation sandstones are slightly enriched in Rb and strongly enriched in Pb whereas mud rocks (shale) are strongly enriched in Rb and Pb. All samples are slightly depleted in Sr and Ba (Fig. 7). Between high field strength elements (HFSE), Zr and Y show slightly enrichment in all samples; however the mud rocks show higher concentrations. Th and Nb are similar to UCC in sandstones but in mud rocks are slightly enriched (Fig. 7). All samples are enriched in U when compared to Upper Continental Crust. The transitional trace elements, such as V, Cr, Cu, Co, Ni and Zn, also show enrichment in all samples when compared to UCC, only V is similar to UCC in sandstones (Fig. 7).

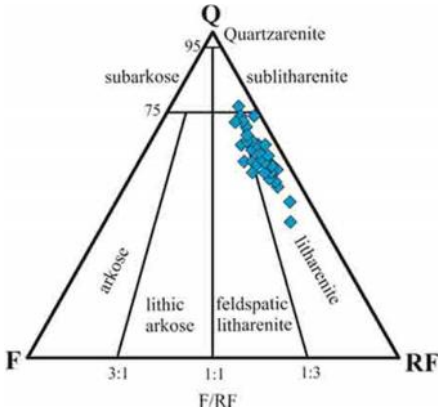


**Figure 4.** Folk [15] triangular diagram shows the classification of Mozduran sandstones.

**Table 3.** Trace element (in ppm) concentrations of sandstone and mudstone samples

| Sample No. | Rb | Sr | Ba | Y | Zr | V | Cr | Co | Ni | Cu | Zn | Th | Pb | U | Nb |
|---|---|---|---|---|---|---|---|---|---|---|---|---|---|---|---|
| SST-Kl-36 | 228 | 235 | 298 | 46 | 852 | 210 | 306 | 53 | 194 | 194 | 389 | 6 | 30 | 14 | 24 |
| SST-Kl-40 | 155 | 177 | 235 | 35 | 219 | 108 | 177 | 64 | 144 | 80 | 102 | 12 | 100 | 7 | 7 |
| SST-K48 | 138 | 162 | 180 | 33 | 219 | 91 | 300 | 42 | 126 | 128 | 141 | 3 | 77 | 12 | 3 |
| SST-Kl-50 | 134 | 165 | 193 | 29 | 200 | 103 | 106 | 52 | 74 | 144 | 255 | 3 | 102 | 6 | 5 |
| SST-K-56 | 162 | 283 | 276 | 44 | 586 | 204 | 261 | 65 | 144 | 129 | 170 | 14 | 57 | 15 | 16 |
| SST-Kl-60 | 187 | 212 | 371 | 52 | 551 | 190 | 279 | 67 | 138 | 127 | 251 | 6 | 89 | 10 | 8 |
| SST-Kl-66 | 164 | 275 | 374 | 36 | 437 | 137 | 202 | 34 | 88 | 98 | 106 | 1 | 33 | 14 | 34 |
| SST-K-20 | 237 | 273 | 599 | 46 | 571 | 220 | 335 | 78 | 174 | 391 | 514 | 17 | 45 | 23 | 78 |
| SST-D-28 | 169 | 1280 | 720 | 34 | 389 | 145 | 166 | 50 | 66 | 136 | 117 | 9 | 20 | 1 | 9 |
| SST-D-35 | 205 | 202 | 312 | 41 | 282 | 121 | 284 | 58 | 95 | 126 | 165 | 7 | 73 | 23 | 4 |
| SST-D-60 | 144 | 162 | 185 | 33 | 244 | 102 | 207 | 42 | 110 | 113 | 146 | 6 | 74 | 3 | 7 |
| SST- K-15 | 179 | 181 | 258 | 49 | 651 | 186 | 242 | 54 | 99 | 208 | 131 | 13 | 44 | 2 | 16 |
| SST-K-25 | 162 | 206 | 209 | 38 | 287 | 119 | 149 | 48 | 117 | 160 | 123 | 11 | 44 | 8 | 6 |
| SST-K-40 | 140 | 160 | 234 | 42 | 400 | 128 | 147 | 40 | 93 | 176 | 124 | 9 | 71 | 9 | 11 |
| SST-K-54 | 100 | 197 | 178 | 31 | 202 | 90 | 144 | 38 | 70 | 107 | 79 | 18 | 25 | 0 | 8 |
| SST- K-59 | 112 | 13 | 144 | 30 | 172 | 85 | 231 | 50 | 88 | 117 | 78 | 6 | 67 | 7 | 8 |
| SST- K-61 | 137 | 146 | 200 | 30 | 273 | 108 | 305 | 48 | 39 | 180 | 140 | 14 | 46 | 17 | 15 |
| SST- K-81 | 97 | 164 | 190 | 31 | 183 | 81 | 124 | 27 | 38 | 175 | 114 | 15 | 53 | 10 | 4 |
| SST- Ko-29 | 27 | 98 | 251 | 16 | 120 | 36 | 173 | 15 | 33 | 155 | 66 | 14 | 74 | 11 | 3 |
| SST- Ko-99 | 64 | 96 | 83 | 24 | 574 | 87 | 345 | 54 | 114 | 171 | 55 | 3 | 36 | 10 | 12 |
| SST- Kl-2 | 162 | 248 | 270 | 41 | 529 | 155 | 338 | 55 | 87 | 166 | 88 | 11 | 138 | 5 | 27 |
| SST- Kl-17 | 130 | 296 | 996 | 35 | 185 | 77 | 135 | 51 | 83 | 145 | 109 | 10 | 108 | 8 | 4 |
| SST- Kl-23 | 133 | 208 | 202 | 34 | 265 | 111 | 222 | 51 | 9 | 158 | 78 | 7 | 76 | 15 | 13 |
| SST-Kl-56 | 77 | 147 | 119 | 33 | 135 | 65 | 93 | 48 | 143 | 143 | 102 | 9 | 97 | 10 | 4 |
| SST-Kl-58 | 144 | 187 | 223 | 39 | 436 | 140 | 323 | 60 | 28 | 134 | 149 | 14 | 108 | 13 | 5 |
| Mean | 143 | 231 | 292 | 36 | 358 | 124 | 224 | 50 | 96 | 154 | 152 | 10 | 67 | 10 | 13 |
| M-Kl-13 | 328 | 302 | 398 | 63 | 635 | 286 | 293 | 114 | 160 | 240 | 387 | 17 | 76 | 15 | 25 |
| M-Kl-14 | 259 | 267 | 302 | 57 | 919 | 195 | 274 | 32 | 31 | 117 | 52 | 19 | 146 | 19 | 30 |
| M-Kl-24 | 372 | 286 | 436 | 63 | 698 | 317 | 307 | 108 | 246 | 174 | 460 | 24 | 96 | 12 | 45 |
| M-Kl-65 | 404 | 338 | 462 | 69 | 677 | 339 | 327 | 96 | 221 | 262 | 854 | 16 | 154 | 17 | 34 |
| M- D-1 | 418 | 415 | 435 | 71 | 655 | 325 | 317 | 136 | 441 | 144 | 205 | 9 | 97 | 18 | 38 |
| M- D-15 | 433 | 334 | 593 | 79 | 515 | 353 | 302 | 127 | 246 | 172 | 270 | 29 | 40 | 8 | 4 |
| M- K-51 | 307 | 228 | 381 | 76 | 1058 | 285 | 293 | 84 | 239 | 139 | 443 | 19 | 76 | 25 | 37 |
| M- Ko-4 | 563 | 242 | 396 | 78 | 542 | 364 | 299 | 103 | 157 | 237 | 315 | 26 | 120 | 14 | 24 |
| M- Ko-49 | 263 | 225 | 347 | 52 | 503 | 297 | 246 | 120 | 263 | 141 | 258 | 14 | 95 | 11 | 36 |
| M- Ko-80 | 546 | 373 | 441 | 80 | 525 | 476 | 380 | 162 | 330 | 145 | 345 | 35 | 113 | 16 | 45 |
| Mean | 389 | 301 | 419 | 69 | 673 | 324 | 304 | 108 | 233 | 177 | 359 | 21 | 101 | 16 | 32 |
| UCC | 112 | 350 | 550 | 22 | 190 | 107 | 83 | 17 | 44 | 25 | 71 | 10.70 | 17 | 2.80 | 12 |

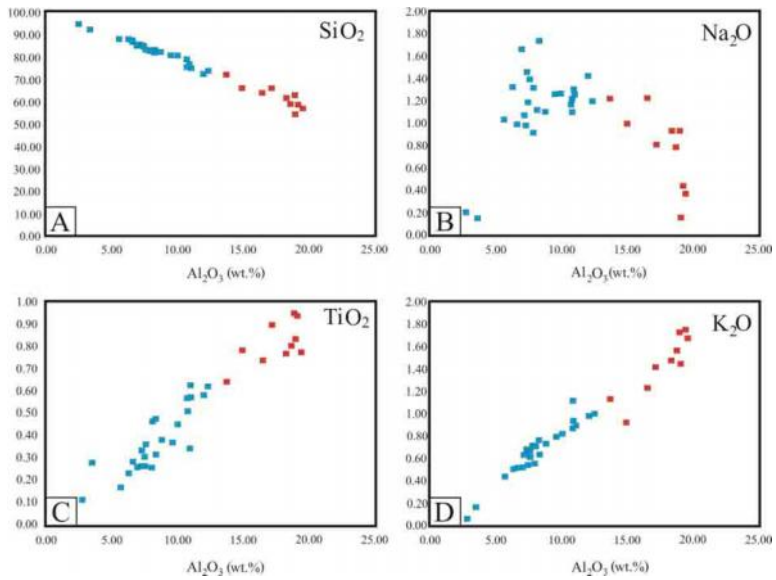


**Figure 5.** Selected major elements versus $Al_2O_3$ variation diagrams for Mozdouran clastic sediments.

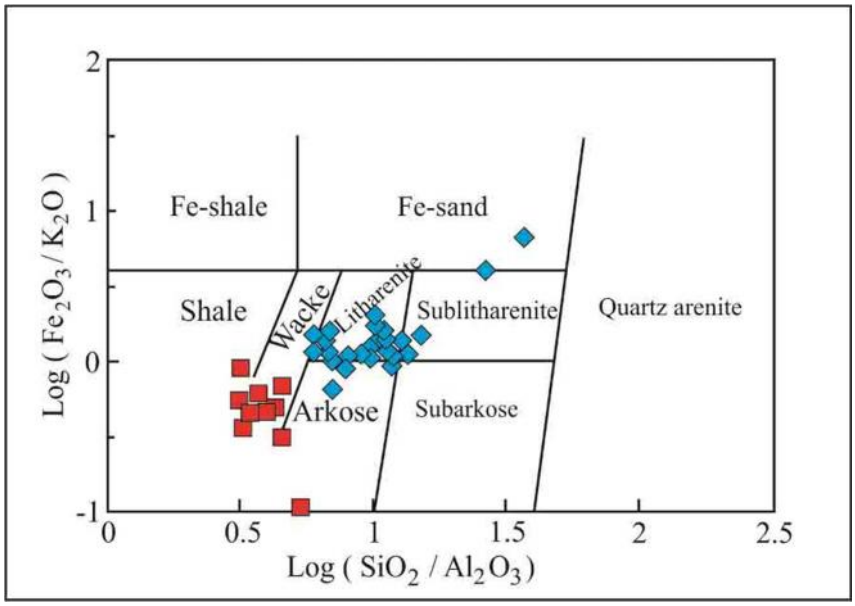


**Figure 6.** Geochemical classification diagram of log ($SiO_2/Al_2O_3$) vs. log($Fe_2O_3/K_2O$) for the Mozduran sandstone samples [17].

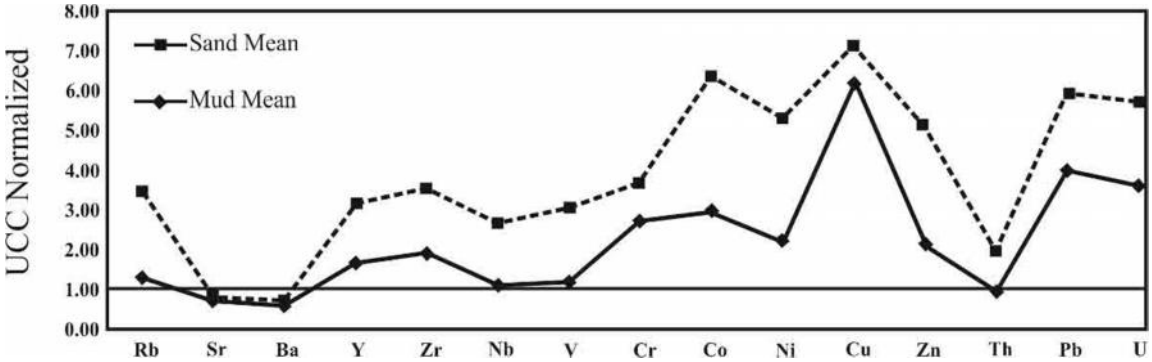


**Figure 7.** UCC normalized trace element distribution patterns of sandstones and mudstones (data from table 3).

## Discussion

In this paper, discussion is focuses on the provenance studies that are divided five section including paleoweathering, hydraulic sorting, parent rock, tectonic setting and paleogeography.

### *1. Source area paleoweathering*

The quality of chemical weathering in siliciclastic sedimentary rocks can be evaluated by inquiring the relationship between alkali and earth alkaline elements [18]. The degree of chemical weathering in sandstones can be estimated by calculating different indices [19, 20]. Between them, chemical index of alteration (CIA) and plagioclase index of alteration (PIA) usually used for interpretation of the source area paleowaethering that are shown in the equations below [18, 21]:

$$CIA= [Al_2O_3/(Al_2O_3+CaO^*+Na_2O+K_2O)]*100$$ and

$$PIA=[(Al_2O_3-K_2O)/(Al_2O_3+CaO^*+Na_2O+K_2O)]*100)$$

Where CaO* represents the Ca in the silicate phases.

The CIA and PIA value for unweathered rocks is 50 and the effects of weathering increases with increasing values of CIA and PIA. The CIA values of the Mozduran sandstones vary from 55.60 to 75.74 with an average value of 64.57 and the CIA values of shales vary from 67.38 to 75.77 with an average of 70.83 (Table 2). The calculated PIA for sandstones range from 57.64 to 84.27 with an average of 71.59 and for shales vary from 75.61 to 96.22 with an average of 85.84. These indices indicate moderate chemical weathering in the source area of the Mozduran sediments and may reflect semiarid climate conditions in the source area [e.g. 18].

### *2. Hydraulic sorting*

Index of geochemical variability (ICV) can be used to evaluate hydraulic sorting [22]. Minerals such as plagioclase, k-feldspar, pyroxenes and amphiboles show ICV index values of >0.84, whereas weathering products such as illite and kaolinite show values of <0.84 [23]. The mean value of the ICV in Mozduran sandstones (0.90) and shales (0.86) are higher than 0.84 (Table 2), indicating that they are not strongly weathered and are enriched in rock forming minerals as seen by the presence of rock fragments in petrography studies similar to what have been stated by Ohta [24] for Jurassic Ashikita Group, south-west Japan.

### *3. Parent rock compositions*

Petrographic studies show that most of the quartz grains in the Mozduran sandstones are monocrystalline, however polycrystalline quartz, such as recrystallized and stretched metamorphic quartz partly with muscovite inclusions, are present. Alkali feldspars are more common than plagioclase that can be related to more stability of alkali feldspars or the lack of plagioclase bearing rocks at the source area. Two types of rock fragments, low grade metamorphic and sedimentary, are present. The geochemistry of siliciclastic rocks can be used as a complementary data for petrographic evidences that are useful for understanding the composition and type of parent rocks [25, 26, 27, 28, 29]. Because of low solubility of Al and Ti during weathering and transport processes [30], the $TiO_2/Al_2O_3$ ratios used to investigate the composition of source rocks (Fig. 8). On $TiO_2/Al_2O_3$ diagram, most of sandstones and shales plotted near intermediate to felsic source rocks. Girty et al. [31] found that an $Al_2O_3/TiO_2$ ratio in the range of 19-28 in sediments is indicative of felsic source rocks. Therefore, high $Al_2O_3/TiO_2$ ratio (>17) in Mozduran sandstones and shales is also support our interpretation of the felsic source rocks for these sediments. This is also verified by plotting of samples in the $TiO_2$ vs. Ni bivariate diagram of Floyd et al. [32] (Fig. 9). Trace element ratios, such as Th/Cr and Th/Co, have also been found to be different in felsic and mafic/ultramafic source rocks [33]. Th/Cr ratio in Mozduran sandstones ranges between 0.005 to 0.125 with an average of 0.050 and in shales varies from 0.028 to 0.096 with an average of 0.068 (Table 4). Th/Cr in sediments originated from felsic and mafic source rocks ranges from 0.13 to 2.7 and 0.018 to 0.046, respectively [23]. Therefore, Th/Cr ratio of the Mozduran samples indicates that they may have probably been derived from mafic source rocks. Th/Co ratio varies from 0.029 to 0.933 in sandstones and from 0.066 to 0.252 in shales of studied samples which indicate derivation from a

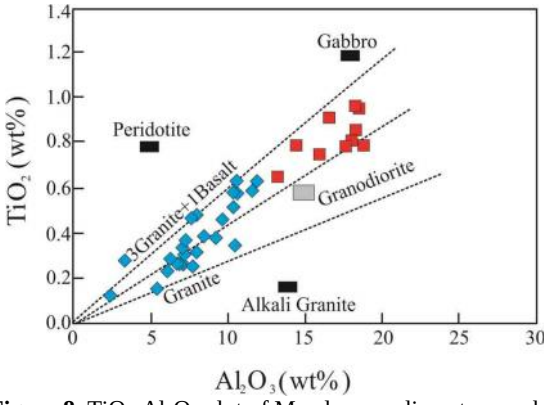


**Figure 8.** $TiO_2$-$Al_2O_3$ plot of Mozduran sedimentary rocks.

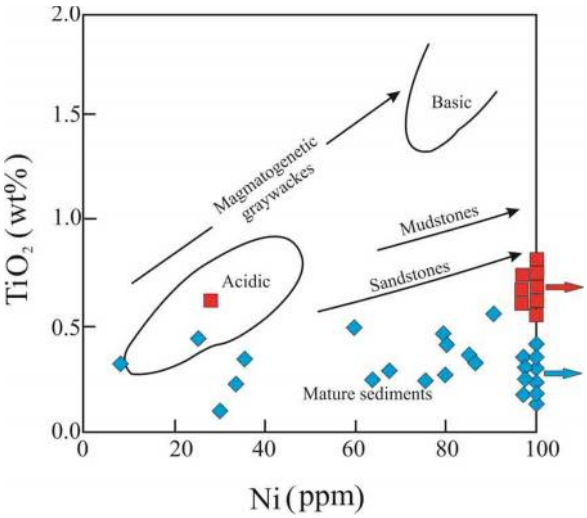


**Figure 9.** $TiO_2$ versus Ni relationship [29] for the Mozduran samples.

mafic source rock, because sediments derived from a mafic source rock have Th/Co ranges between 0.04 to 1 [23]. Garver et al. [34] found that the Cr/Ni ratio in sandstones from an ultramafic source was greater than 3.0 but most of the Mozduran sandstones and shales have Cr/Ni ratio of less than 3.0 except 4 sandstone (SST-KR201, SST-KR243, SST-N599 and SST-N611) and one shale samples (M-K14). Therefore, based on geochemical analyses of sandstones and shales, these rocks may have derived from both felsic and mafic source areas.

### *4. Tectonic setting*

QtFL and QmFLt ternary diagrams for sandstone are usually applied to show the relationship between sandstone composition and major provenance types, such as stable cratons, basement uplifts, magmatic arcs and recycled orogens [35]. For interpretation of the tectonic setting of Mozduran sandstone, based on petrography, data were plotted on the QtFL and QmFLt

**Table 4.** Selected ratios of trace elements of sandstone and mudstone samples from the Mozduran Formation.

| Sample No. | Th/U | Th/Co | Cr/Zr | Ni/Co | V/Ni | Th/Cr | Cr/Ni | Cr/V | Y/Ni |
|---|---|---|---|---|---|---|---|---|---|
| SST-Kl-36 | 0.43 | 0.11 | 0.36 | 3.66 | 1.08 | 0.020 | 1.58 | 1.46 | 0.24 |
| SST-Kl-40 | 1.71 | 0.19 | 0.81 | 2.25 | 0.75 | 0.068 | 1.23 | 1.64 | 0.24 |
| SST-K48 | 0.25 | 0.07 | 1.37 | 3.00 | 0.72 | 0.010 | 2.38 | 3.30 | 0.26 |
| SST-Kl-50 | 0.50 | 0.06 | 0.53 | 1.42 | 1.39 | 0.028 | 1.43 | 1.03 | 0.39 |
| SST-K-56 | 0.93 | 0.22 | 0.45 | 2.22 | 1.42 | 0.054 | 1.81 | 1.28 | 0.31 |
| SST-Kl-60 | 0.60 | 0.09 | 0.51 | 2.06 | 1.38 | 0.022 | 2.02 | 1.47 | 0.38 |
| SST-Kl-66 | 0.07 | 0.03 | 0.46 | 2.59 | 1.56 | 0.005 | 2.30 | 1.47 | 0.41 |
| SST-K-20 | 0.74 | 0.22 | 0.59 | 2.23 | 1.26 | 0.051 | 1.93 | 1.52 | 0.26 |
| SST-D-28 | 9.00 | 0.18 | 0.43 | 1.32 | 2.20 | 0.054 | 2.52 | 1.14 | 0.52 |
| SST-D-35 | 0.30 | 0.12 | 1.01 | 1.64 | 1.27 | 0.025 | 2.99 | 2.35 | 0.43 |
| SST-D-60 | 2.00 | 0.14 | 0.85 | 2.62 | 0.93 | 0.029 | 1.88 | 2.03 | 0.30 |
| SST- K-15 | 6.50 | 0.24 | 0.37 | 1.83 | 1.88 | 0.054 | 2.44 | 1.30 | 0.49 |
| SST-K-25 | 1.38 | 0.23 | 0.52 | 2.44 | 1.02 | 0.074 | 1.27 | 1.25 | 0.32 |
| SST-K-40 | 1.00 | 0.23 | 0.37 | 2.33 | 1.38 | 0.061 | 1.58 | 1.15 | 0.45 |
| SST-K-54 | 18.00 | 0.47 | 0.71 | 1.84 | 1.29 | 0.125 | 2.06 | 1.60 | 0.44 |
| SST- K-59 | 0.86 | 0.12 | 1.34 | 1.76 | 0.97 | 0.026 | 2.63 | 2.72 | 0.34 |
| SST- K-61 | 0.82 | 0.29 | 1.12 | 0.81 | 2.77 | 0.046 | 7.82 | 2.82 | 0.77 |
| SST- K-81 | 1.50 | 0.56 | 0.68 | 1.41 | 2.13 | 0.121 | 3.26 | 1.53 | 0.82 |
| SST- Ko-29 | 1.27 | 0.93 | 1.44 | 2.20 | 1.09 | 0.081 | 5.24 | 4.81 | 0.48 |
| SST- Ko-99 | 0.30 | 0.06 | 0.60 | 2.11 | 0.76 | 0.009 | 3.03 | 3.97 | 0.21 |
| SST- Kl-2 | 2.20 | 0.20 | 0.64 | 1.58 | 1.78 | 0.033 | 3.89 | 2.18 | 0.47 |
| SST- Kl-17 | 1.25 | 0.20 | 0.73 | 1.63 | 0.93 | 0.074 | 1.63 | 1.75 | 0.42 |
| SST- Kl-23 | 0.47 | 0.14 | 0.84 | 0.18 | 12.33 | 0.032 | 24.67 | 2.00 | 3.78 |
| SST-Kl-56 | 0.90 | 0.19 | 0.69 | 2.98 | 0.45 | 0.097 | 0.65 | 1.43 | 0.23 |
| SST-Kl-58 | 1.08 | 0.23 | 0.74 | 0.47 | 5.00 | 0.020 | 11.54 | 2.31 | 1.39 |
| Mean | 1.00 | 0.20 | 0.63 | 1.92 | 1.29 | 0.050 | 2.33 | 1.81 | 0.38 |
| M-Kl-13 | 1.13 | 0.15 | 0.46 | 1.40 | 1.79 | 0.058 | 1.83 | 1.02 | 0.39 |
| M-Kl-14 | 1.00 | 0.59 | 0.30 | 0.97 | 6.29 | 0.069 | 8.84 | 1.41 | 1.84 |
| M-Kl-24 | 2.00 | 0.22 | 0.44 | 2.28 | 1.29 | 0.078 | 1.25 | 0.97 | 0.26 |
| M-Kl-65 | 0.94 | 0.17 | 0.48 | 2.30 | 1.53 | 0.049 | 1.48 | 0.96 | 0.31 |
| M- D-1 | 0.50 | 0.07 | 0.48 | 3.24 | 0.74 | 0.028 | 0.72 | 0.98 | 0.16 |
| M- D-15 | 3.63 | 0.23 | 0.59 | 1.94 | 1.43 | 0.096 | 1.23 | 0.86 | 0.32 |
| M- K-51 | 0.76 | 0.23 | 0.28 | 2.85 | 1.19 | 0.065 | 1.23 | 1.03 | 0.32 |
| M- Ko-4 | 1.86 | 0.25 | 0.55 | 1.52 | 2.32 | 0.087 | 1.90 | 0.82 | 0.50 |
| M- Ko-49 | 1.27 | 0.12 | 0.49 | 2.19 | 1.13 | 0.057 | 0.94 | 0.83 | 0.20 |
| M- Ko-80 | 2.19 | 0.22 | 0.72 | 2.04 | 1.44 | 0.092 | 1.15 | 0.80 | 0.24 |
| Mean | 1.31 | 0.19 | 0.45 | 2.16 | 1.39 | 0.068 | 1.30 | 0.94 | 0.30 |
| UCC | 3.82 | 0.63 | 0.44 | 2.59 | 2.43 | 0.13 | 1.89 | 0.78 | 0.50 |

ternary diagrams of Dickinson et al. [35]. Our samples are plotted on the recycled orogenic fields (Fig. 10). Such recycled orogenic tectonic discrimination filed

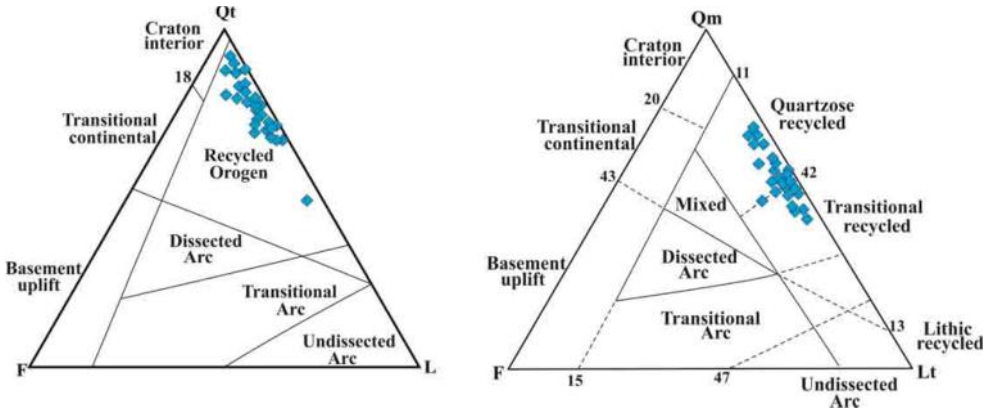


**Figure 10.** QtFL and QmFLt ternary diagrams for the Mozduran Formation sandstones after Dickinson et al. [35].

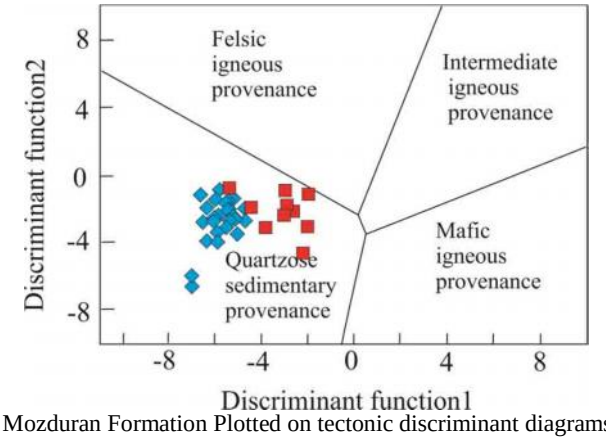


**Figure 11.** Samples of the Mozduran Formation Plotted on tectonic discriminant diagrams of Roser and Korsch [36].

reflects recycled sands from a passive continental margin [35] that is also verified by plotting the samples in the discrimination diagram of Roser and Korsch [36]

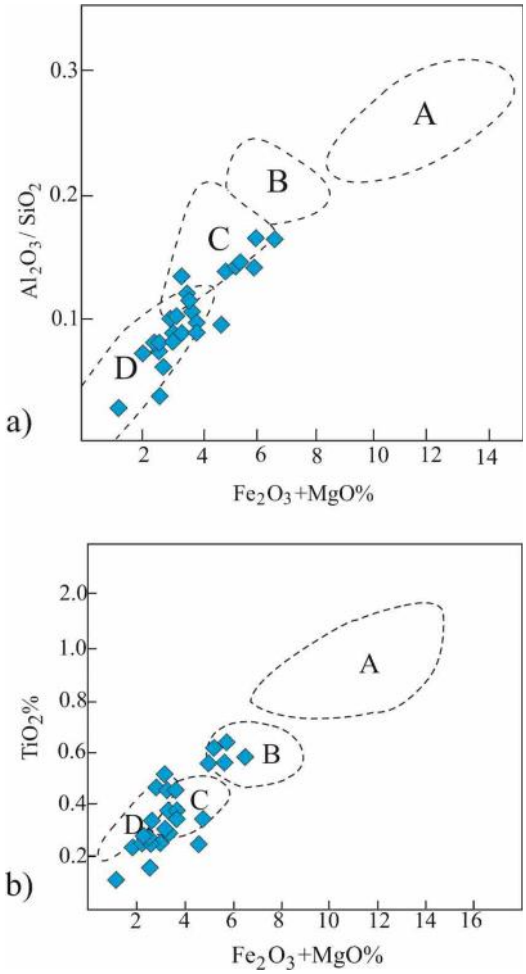


**Figure 12.** Discriminant diagrams for tectonic settings based on major element values after Bhatia [37]. (a) $Fe_2O_3$+MgO vs. $Al_2O_3/SiO_2$; (b) $Fe_2O_3$+MgO vs. $TiO_2$.

(Fig. 11). The possible tectonic settings of the Mozduran Formation also evaluated by geochemical data by using diagrams of Bhatia [37] and Kroonenberg [38]. In the $Al_2O_3/SiO_2$ vs. $Fe_2O_3$+MgO as well as $TiO_2$ vs. $Fe_2O_3$+MgO diagrams of Bhatia [37], samples mostly plotted in a passive continental margin (Fig. 12). In the triangular diagram of Kroonenberg [38], the sandstones plotted on the passive continental margin, however, the shale samples plotted near the boundary of passive and active continental margins (Fig. 13). Furthermore, two discrimination function diagrams for tectonic discrimination of siliciclastic sediments Verma and Armstrong-Altrin [39] have been used: one for high-silica rocks [$(SiO_2)$adj = 63 % to 95 %] and one for low-silica [$(SiO_2)$adj = 35 % to 63 %]. These discrimination diagrams differentiate among tectonic settings such as island or continental arc (Arc), continental rift (Rift), and collision (Col) settings. According to $SiO_2$ content of the Mozduran samples, the tectonic discrimination diagram for high and low silica have been used. Two discrimination functions (F1 and F2) are calculated based on major element concentrations (Fig. 14). The results obtained from discriminant functions analysis provide strong evidence of deposition in a rift basin, as stated by Afshar-Harb [1] and Robert et al. [10] (Fig. 14).

### *5. Paleogeography perspective*

Most of the researchers are believed that the Kopet-Dagh Basin is the southern edge of Turan plate and in fact a part of Eurasian super continent at most of the times [11, 40] (Fig. 15). Fine grained turbidites, radiolarite, chert, pillow lavas and ultramafic rocks from the east of Sefidsang village (southeast of Mashhad) with the Late Permian age show that an intracontinental rift was created during the Late Carboniferous and Early Permian time in the northeastern parts of Iran (e.g., [41]). During the latest Triassic-Early Jurassic times,

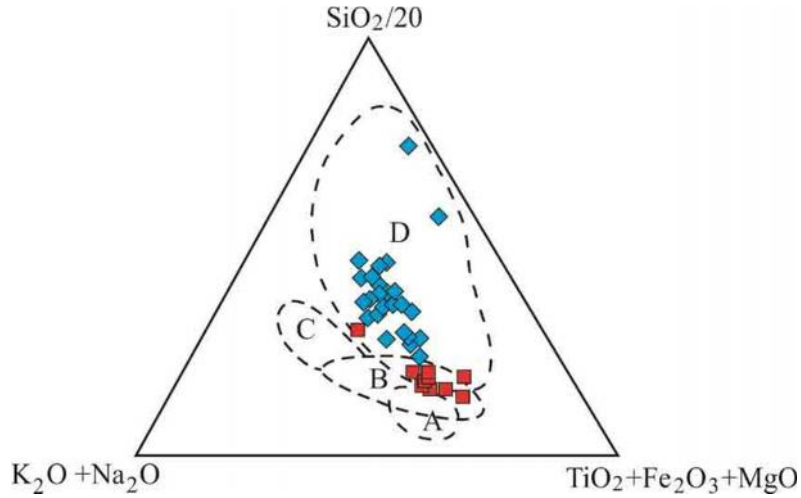


**Figure 13.** Tectonic discrimination ternary plots of Kroonenberg [38] for Mozduran Formation samples.

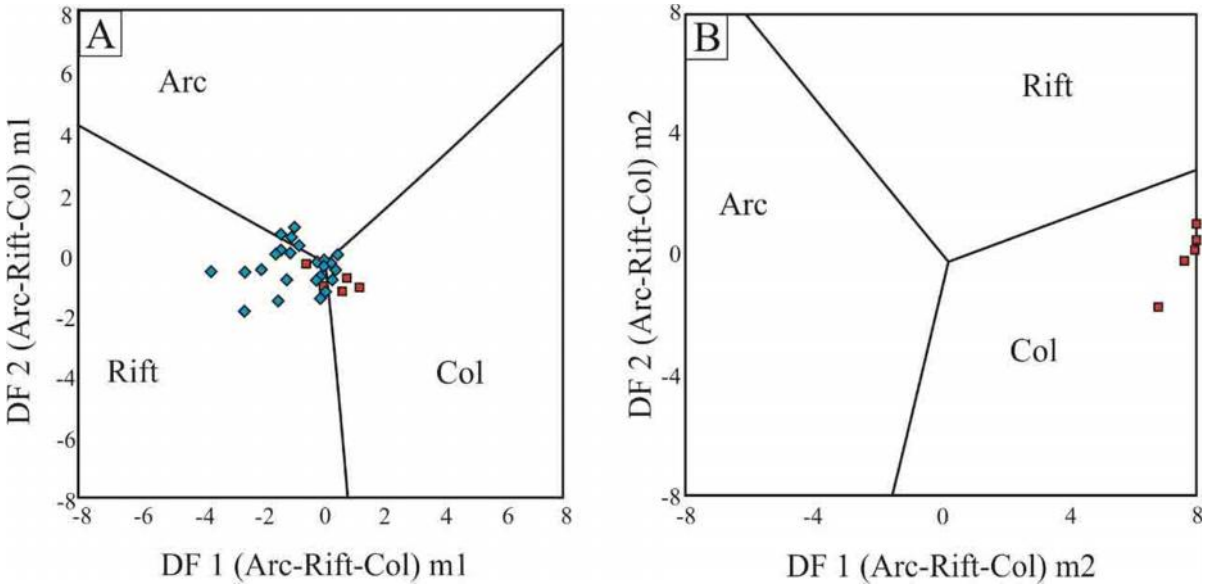


**Figure 14.** Discriminant function diagram proposed by Verma and Armstrong-Altrin [39] for high silica (A) and low silica (B) siliciclastic sediments of the Mozduran Formation from three tectonic settings (arc, continental rift, and collision).

the collision between Iran and Turan palates (Cimmerian Orogeny) occurred [42]. After this orogeny, a rifting phase (Neotethys back-arc rifting) took place north of the Paleotethys suture line in the Mid- Jurassic time [10, 43] and the silisiclastic Kashafrud Formation deposited in horst and graben (block faulting) of the rift system in the Kopet-Dagh Basin. This rifting system developed through the South Caspian Sea in the west (see [10, 40]) and probably into easternmost parts of Iran (Kopet-Dagh Basin) and northwest of Afghanistan, along of Paleotethys suture line (Fig. 15). At this time, the study area was located at the northern Paleotethys suture (south of Aghdarband window in SE Kopet-Dagh Basin) on the northern Iran plate. Transgression in the Early Oxfordian time caused the deposition of Mozduran Formation with erosional boundary on the syn-rift deposits of Kashafrud Formation (see [6]). The silisiclastics facies in the study area, in contrast to carbonates in other parts of the basin, together with decreases in the thickness of the Mozduran Formation toward the easternmost parts of the Kopet-Dagh Basin suggest paleohighs (horst systems) in the eastern part. Therefore, siliciclastic sediments may have been sourced from south and southeast of the study area, especially from the Late Paleozoic to Triassic successions that have been uplifted along the suture line of Paleotethys. Quartzolithic petrofacies of Mozduran sandstones and their

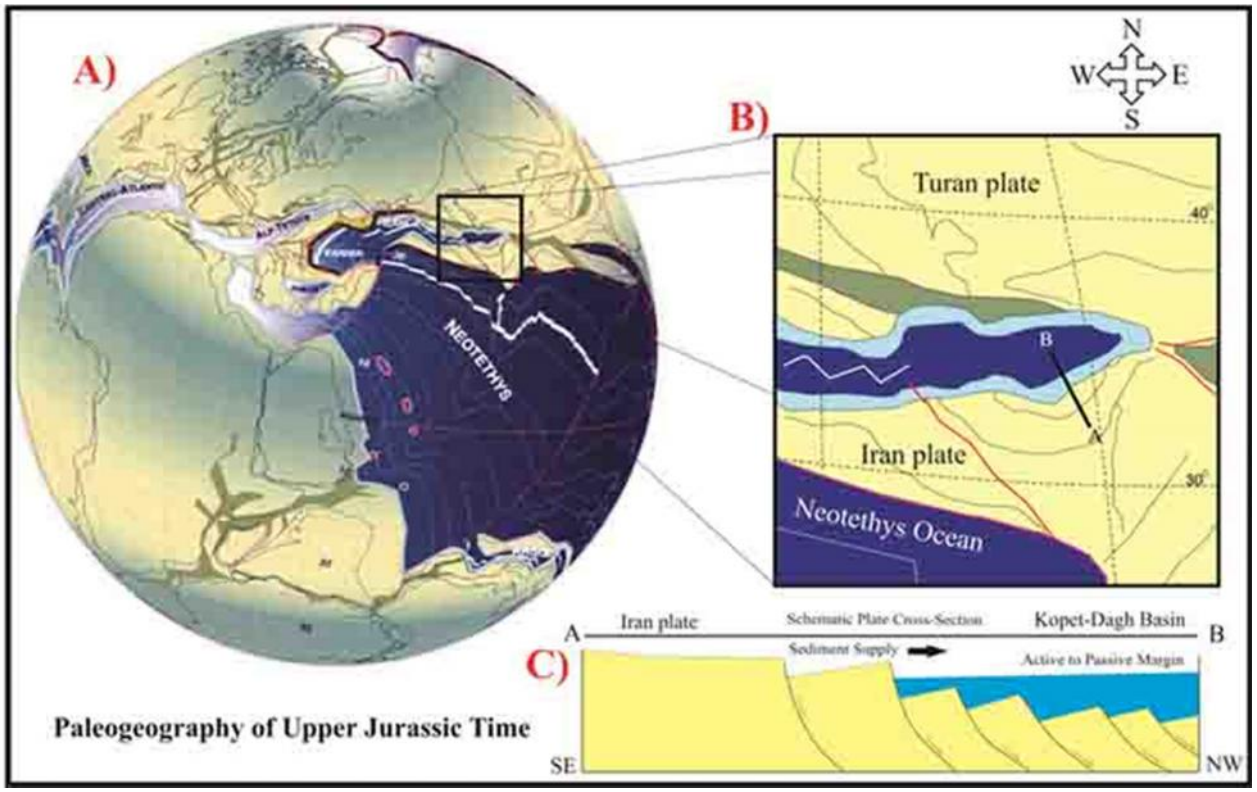


**Figure 15.** A) Schematic reconstruction of paleogeography map of the Late Jurassic time (modified from Stampfli and Borel [41]). B) Close-up view of region that centered on ocean between Iran and Turan plates of figure A during Late Jurassic time. C) Proposed model for deposition of the Upper Jurassic Mozduran Formation in the study area as post rift deposits.

constituents, such as Qp, Qm, Ls, Lm and F, as well as paleocurrent analysis (southeast to northwest) [6]) show that these sediments may have been derived from uplifted sedimentary or sedimentary metamorphic strata from fold-thrust belts of south Mashhad and north of Fariman region.

In the Kopet-Dagh Basin, Mozduran Formation is mainly the youngest lithostratigraphic carbonate unit in Jurassic time. Adabi and Rao [44] showed that the temperature at the time of Mozduran carbonate deposits was about 25 Celiosious which is corresponding with tropical climatic condition. The mean value of CIA for Mozduran sandstone is 64.59 and for shale is 70.83. These values confirm a medium weathering for Mozduran sandstone and shale that can be supported by paleogeography maps (see [10, 40, 43]) as well as temperature obtained from Mozduran dolomites by Adabi and Rao [44]. This moderate value of weathering can be due to semi-arid climatic conditions in the source area that is confirmed by moderate alteration of feldspars in these sandstones. The tectonic setting of Mozduran Formation based on petrographic and geochemical analysis confirmed a continental rifting systems (Fig. 15). Since the Kopet-Dagh Basin is an intracontinental basin in a probably passive continental margin, then the siliciclastic sediments from south and southeast was entered into the basin and deposited along coastal environments of the Jurassic sea (e.g., [2, 6]).

***Conclusions***

Based on Petrographic observations, the sandstones of Mozduran Formation are mostly classified into two types: litharenite and feldspathic litharenite. The average CIA values for the Mozduran sandstones and shales are 64.57 and 70.83 respectively. These values suggest medium weathering that can be due to semi-arid climatic condition in the source area. The average ICV value of Mozduran sandstones (0.90) and shales (0.86) are higher than 0.84, indicating that they are not strongly weathered. Geochemical analyses show that these sediments derived from both felsic and mafic source areas. QtFL and QmFLt ternary diagrams show that the Mozduran sandstones are plotted in recycled orogenic fields. The results of discriminant function analysis provide important evidence of deposition in a rift basin. Petrographic and geochemical analyses suggest that these sediments deposited in a passive tectonic margin. The composition of source rocks together with paleocurrent analysis indicate that they may have been derived from uplifted sedimentary-

metamorphic rocks from south of Mashhad and north of Fariman region.

## Acknowledgment

This study was financially and logistically supported by the Geology Department at the Ferdowsi University of Mashhad (4562). The authors would like to thank the editor and reviewers for useful comments that resulted in a significant improvement in the presentation of this paper.

## References

1. Afshar-Harb A. The stratigraphy, tectonics and petroleum geology of the Kopet Dagh region, northern Iran. Ph.D thesis, Imperial College of Science and Technology, London, 316p (1979).
2. Kavoosi M., Lasemi Y., Sherkati S., and Moussavi-Harami S. R. Facies analysis and depositional sequences of the Upper Jurassic Mozduran Formation, a reservoir in the Kopet Dagh Basin, NE Iran. *J. Petrol. Geol.,* **32**: 235–260 (2009).
3. Adabi M.H. Multistage dolomitization of Upper Jurassic Mozduran Formation, Kopeh-Dagh Basin, N.E. Iran. *Carbonates Evaporites*, **24**: 16–32 (2009).
4. Mahboubi A., Moussavi-Harami S. R., Aghaei A., Carpenter S. J., and Collins L. Petrographical and geochemical evidences for paragenetic sequence interpretation of diagenesis in mixed siliciclastic–carbonate sediments: Mozduran Formation (Upper Jurassic), south of Agh-Darband, NE Iran. *Carbonates Evaporates*, **25**: 231–246 (2010).
5. Kavoosi M. Inorganic control on original carbonate mineralogy and creation of gas reservoir of the Upper Jurassic carbonates in the Kopet-Dagh Basin, NE, Iran. *Carbonates Evaporites*, **29**: 419–432 (2014).
6. Zand-Moghadam H., Moussavi Harami S. R., Mahboubi A., and Aghaei A. Lithofacies and sequence stratigraphic analysis of the Upper Jurassic siliciclastics in the eastern Kopet-Dagh Basin, NE Iran. *J. Afr. Earth Sci.,* **117**: 48–61 (2016).
7. Metcalf K., and Kapp P. The Yarlung suture mélange, Lopu Range, southern Tibet: Provenance of sandstone blocks and transition from oceanic subduction to continental collision. *Gondwana Res.*, **48**: 15-33 (2017).
8. Basu A., Bickford M.E., and Deasy R. Inferring tectonic provenance of siliciclastic rocks from their chemical compositions: A dissent. *Sediment. Geol.*, **336:** 26-35 (2016).
9. Purevjav N., and Roser B. Geochemistry of Silurian–Carboniferous sedimentary rocks of the Ulaanbaatar terrane, Hangay–Hentey belt, central Mongolia:Provenance, paleoweathering, tectonic setting, and relationship with the neighbouring Tsetserleg terrane. *Chem. Erde.*, **73**: 481–493 (2013).
10. Robert A.M.M., Letouzey J., Kavoosi M.A., Sherkati S., Muller C., Verg_ees J., and Aghababae A. Structural evolution of the Kopet Dagh fold-and-thrust belt (NE Iran) and interactions with the South Caspian Sea Basin and Amu Darya Basin. *Mar. Petrol. Geol.*, **57**: 68-87 (2014).
11. Shafaii Moghadam H., Li X.H., Ling X.X., Stern R.J., Khedr M.Z., Chiaradia M., Ghorbani Gh., Arai Sh., and Tamura A. Devonian to Permian evolution of the Paleo-Tethys Ocean: New evidence from U-Pb zircon dating and Sr-Nd-Pb isotopes of the Darrehanjir- Mashhad "ophiolites", NE Iran. *Gondwana Res.*, **28 (2):** 781-799 (2015).
12. Shafaii Moghadam H., and Stern R.J. Ophiolites of Iran: Keys to understanding the tectonic evolution of SW Asia: I) Paleozoic ophiolites. *J. Asian Earth Sci.*, **100:** 31-59 (2015).
13. Taheri J., Fürsich F., and Wilmsen M. Stratigraphy, depositional environments and geodynamic significance of the Upper Bajocian Bathonian Kashafrud Formation, NE Iran. in: Brunet M. F., Wilmsen M., Granath J.W. (Eds.), South Caspian to Central Iran Basins. *Geol. Soc. London., Spec. Public.*, **312**: pp. 205–218 (2009).
14. Sardar Abadi M., Da Silva A.C., Amini A., Boulvain F., and Sardar Abadi M.H. Tectonically controlled sedimentation: impact on sediment supply and basin evolution of the Kashafrud Formation (Middle Jurassic, Kopeh-Dagh Basin, northeast Iran. *Int. J. Earth Sci.,* **103**: 2233–2254 (2014).
15. Folk R.L. Petrology of Sedimentary Rocks. *Hemphill Publication Company, Austin*, 182 p (1980).
16. Harker A. The natural history of igneous rocks, Macmillan, New York, 384p (1909).
17. Herron M.M. Geochemical classification of terrigenous sands and shales from core or log data. *J. Sedimet. Petrol.,* **58**: 820–829 (1988).
18. Nesbitt H.W., and Young G.M., 1982. Early Proterozoic climate and plate motions inferred from major elements chemistry of lutites. *Nature*, **299**: 715–717 (1982).
19. Shao J., Yang Sh., and Li Ch. Chemical indices (CIA and WIP) as proxies for integrated chemical weathering in China: Inferences from analysis of fluvial sediments. *Sediment. Geol.*, **265–266**: 110-120 (2012).
20. Garzanti E., and Resentini A. Provenance control on chemical indices of weathering (Taiwan river sands). *Sediment. Geol.*, **336**: 81-95 (2016).
21. Fedo C.M., Nesbitt H.W., and Young G.M. Unraveling the effects of potassium metasomatism in sedimentary rocks and paleosols, with implications for paleoweathering conditions and provenance. *Geology*, **23**: 921–924 (1995).
22. Perri F. Composition, provenance and source weathering of Mesozoic sandstones from Western-Central Mediterranean Alpine Chains. J. *Afr. Earth Sci.*, **91**, 32-43 (2014).
23. Armstrong-Altrin J.S., and Machain-Castillo M. L. Mineralogy, geochemistry, and radiocarbon ages of deep sea sediments from the Gulf of Mexico, Mexico. *J. S. Am. Earth Sci.*, **71**: 182-200, (2016).
24. Ohta T. Measuring and adjusting the weathering and hydraulic sorting effect for rigorous provenance analysis of sedimentary rocks: a case study from the Jurassic Ashikita Group, south-west Japan. *Sedimentology*, **55**: 1687-1701 (2008).

25. Zaid S. M. Provenance, diagenesis, tectonic setting and geochemistry of Rudies sandstone (Lower Miocene), Warda Field, Gulf of Suez, Egypt. *J. Afr. Earth Sci.*, **66–67**: 56–71 (2012).
26. Pantopoulos G., and Zelilidis A. Petrographic and geochemical characteristics of Paleogene turbidite deposits in the southern Aegean (Karpathos Island, SE Greece): Implications for provenance and tectonic setting. *Chem. Erde.*, **72**: 153–166 (2012).
27. Zand-Moghadam H., Moussavi-Harami R., Mahboubi A., and Rahimi B. Petrography and geochemistry of the Early-Middle Devonian sandstones of the Padeha Formation the north of Kerman, SE Iran: Implication for provenance. *Boletín del Instituto de Fisiografía y Geología,* **83**: 1-14 (2013).
28. Jafarzadeh M., Moussavi-Harami S. R., Amini A., Mahboubi A., and Farzaneh F. Geochemical constraints on the provenance of Oligocene–Miocene siliciclastic deposits (Zivah Formation) of NW Iran: implications for the tectonic evolution of the Caucasus. *Arab. J. Geosci.*, **7**: 4245-4263 (2014).
29. Castillo P., Lacassie J. P., Augustsson C., and Hervé F. Petrography and geochemistry of the Carboniferous-Triassic Trinity Peninsula Group, West Antarctica: Implications for provenance and tectonic setting. *Geol. Mag.*, **152**: 575–588 (2015).
30. Hu J., Li Q., Fang N., and Yang J, Ge D. Geochemistry characteristics of the Low Permian sedimentary rocks from central uplift zone, Qiangtang Basin, Tibet: insights into source-area weathering, provenance, recycling, and tectonic setting. *Arab. J. Geosci.*, **8**:5373–5388, (2015).
31. Girty G.H., Ridge D.L., Knaack C., Johnson D., and Al-Riyami R.K. Provenance and depositional setting of Paleozoic Chert and Argillite, Sierra Nevada, California. *J. Sediment. Res.*, **66**: 107–118 (1996).
32. Floyd P.A., Winchester J.A., and Park R.G. Geochemistry and tectonic setting of Lewisianclastic metasediments from the Early Proterozoic Loch Maree Group of Gairloch, N.W. Scotland. *Precambrian Res.*, **45**: 203–214 (1989).
33. Armstrong-Altrin J.S., Lee Y.I., Kasper-Zubillaga J.J., Carranza-Edwards A., Garcia D., Eby, N., Balaram V., and Cruz-Ortiz N.L. Geochemistry of beach sands along the western Gulf of Mexico, Mexico: implication for provenance. *Chem. Erde.*, **72**: 345–362 (2012).
34. Garver J.I., Royce P.R., and Smick T.A. Chromium and nickel in shale of the Taconic Foreland: a case study for the provenance of fine-grained sediments with an ultramafic source. *J. Sediment. Res.*, **66**: 100–106 (1996).
35. Dickinson W.R., Beard L.S., Brakenridge G.R., Evjavec J.L., Ferguson R.C., Inman K.F., Knepp R.A., Lindberg F.A., and Ryberg P.T. Provenance of North American Phanerozoic sandstones in relation to tectonic setting. *Geol. Soc. Am. Bull.*, **94**: 222–235 (1983).
36. Roser B.P., and Korsch R.J. Provenance signatures of sandstone–mudstone suites determined using discriminant function analysis of major-element data. *Chem. Geol.*, **67**: 119–139 (1988).
37. Bhatia M. R. Plate tectonics and geochemical composition of sandstones. *J. Geol.*, **91**: 611–627 (1983).
38. Kroonenberg S.B. Effects of provenance, sorting and weathering on the geochemistry of fluvial sands from different tectonic and climatic environments. in: Proceedings of the 29th International Geological Congress, Part A, Kyoto, Japan 1992, Kumon F. and Yu K.M. (Eds.), *V.S.P. Public., Utrecht.*, pp. 69–81 (1994).
39. Verma S.P., and Armstrong-Altrin J.S. New multi-dimensional diagrams for tectonic discrimination of silica clastic sediments and their application to Pre-Cambrian basins. *Chem. Geol.*, **355**: 117-180 (2013).
40. Stampfli G.M., and Borel G.D. A plate tectonic model for the Paleozoic and Mesozoic constrained by dynamic plate boundaries and restored synthetic oceanic isochrons. *Earth Planet. Sci. Lett.*, **196**: 17–33 (2002).
41. Agard P., Omrani J., Jolivet L., Whitechurch H., Vrielynck B., Spakman W., Monié P., Meyer B., and Wortel R. Zagros orogeny: a subduction-dominated process. *Geol. Mag.*, **148** (5-6): 692-725 (2011).
42. Zanchetta S., Berra F., Zanchi A., Bergomi M., Caridroit,M., Nicorab A., and Heidarzadeh G. The record of the Late Palaeozoic active margin of the Palaeotethys in NE Iran: constraints on the Cimmerian orogeny. *Gondwana Res.*, **24** (3-4): 1237-1266 (2013).
43. Wilmsen M., Fürsich T., Emami K.S., Majidifard M.R., and Taheri M.R. The Cimmerian Orogeny in northern Iran: tectono-stratigraphic evidence from the foreland. *Terra Nova*, **21** (3): 211-218 (2009).
44. Adabi M.H., and Rao C.P. Petrographic and geochemical evidence for original aragonite mineralogy of Upper Jurassic Carbonates (Mozduran Formation), Sarakhs area, Iran. *Sediment. Geol*., **72**: 253–267 (1991).